

# Proton emission induced by polarized photons

M. Anguiano<sup>1</sup>, G. Co' <sup>2,3</sup> and A.M. Lallena<sup>1</sup>

<sup>1)</sup> *Departamento de Física Atómica, Molecular y Nuclear,  
Universidad de Granada, E-18071 Granada, Spain*

<sup>2)</sup> *Dipartimento di Fisica, Università di Lecce, I-73100 Lecce, Italy*

<sup>3)</sup> *Istituto Nazionale di Fisica Nucleare sez. di Lecce, I-73100 Lecce, Italy*

(Dated: June 4, 2017)

The proton emission induced by polarized photons is studied in the energy range above the giant resonance region and below the pion emission threshold. Results for the  $^{12}\text{C}$ ,  $^{16}\text{O}$  and  $^{40}\text{Ca}$  nuclei are presented. The sensitivity of various observables to final state interaction, meson exchange currents and short range correlations is analyzed. We found relevant effects due to the virtual excitation of the  $\Delta$  resonance.

PACS numbers: 25.20.-x, 25.20.Lj

## I. INTRODUCTION

In a previous work [1] we have investigated the sensitivity of the  $(\gamma, p)$  reactions to short range correlations (SRC), meson-exchange currents (MEC) and final state interactions (FSI). The SRC are related to the short-distance repulsion of the nucleon-nucleon potential [2, 3]. The search for SRC effects in nuclear systems is done by studying deviations from mean field results [4, 5]. The exchange of mesons between interacting nucleons produces electromagnetic currents called MEC. Effects related to the MEC have been clearly identified in few-body systems [6, 7]. In heavier nuclei, however, a clean identification of MEC effects is hidden, to a large extent, by the uncertainties of the nuclear wave function [8]. The FSI account for the re-interaction of the emitted nucleon with the remaining nucleus. A successful approach to describe nucleon emission data induced by both electrons and photons [9, 10], treats the FSI with an optical potential whose parameters are fixed to reproduce elastic nucleon-nucleus scattering data.

Almost all the experimental work relative to the photo-emission of a single proton in medium-heavy nuclei, has been done with unpolarized photons [11]. We are aware of only two experiments of  $(\vec{\gamma}, p)$  type. In the first one, Wienhard *et al.* [12] studied the  $^{16}\text{O}(\vec{\gamma}, p)^{15}\text{N}$  reactions in the giant resonance region by using photons with energies between 15 and 25 MeV. In the other experiment, Yokokawa *et al.* [13] used as a target the  $^{12}\text{C}$  nucleus and the photon energies varied between 40 and 70 MeV.

The recent development of tagged photon facilities opens new perspectives for this type of experiments. For example the Mainz Microtron (MAMI) [14] and the new tagged photon beam line at MAX-laboratory, in Lund [15], can make experiments with polarized photons and produce data with a high energy resolution. This allows a clear separation of the different states of the residual nucleus [16]. At MAMI, polarized photon beams have been already used to study  $^{12}\text{C}(\vec{\gamma}, pd)$ ,  $^{12}\text{C}(\vec{\gamma}, pp)$  and  $^{12}\text{C}(\vec{\gamma}, pm)$  reactions [17]. At MAX-laboratory two experiments with polarized photons have been proposed. In the first one, linearly polarized bremsstrahlung photons will be used to make Compton scattering on  $^4\text{He}$  and  $^{12}\text{C}$  nuclei. In the second experiment cross sections and asymmetries of the two-particle photodisintegration of  $^6\text{Li}$  and  $^7\text{Li}$  nuclei will be measured. Another experimental facility which produces polarized gamma-ray beams is HIGS, at the Duke University in Durham [18], where the first measurements of the  $^2\text{H}(\vec{\gamma}, n)p$  analyzing power near threshold have been done [19].

The experimental situation is rapidly evolving and the possibility of using polarized photons to study the structure of medium-heavy nuclei is a solid perspective. In this work we study this possibility from the theoretical point of view, by using a nuclear model recently developed to investigate electromagnetic excitations of the nucleus in inclusive [20, 21, 22, 23], single [1, 24] and double coincidence [25, 26] experiments. The starting point of our approach is the continuum shell model implemented with the optical potential to take into account the FSI. By using this model to describe nuclear excited states we treat the MEC by considering one-pion exchange diagrams [27, 28, 29]. We improve this picture by implementing the SRC acting on one-body electromagnetic currents. The SRC are considered by calculating all the diagrams containing a single correlation line. The validity of this approach has been verified in Ref. [21] by comparing nuclear matter charge responses obtained with our model and with a full Correlated Basis Function calculation.

In our previous investigation [1] we found that photoemission cross sections have a greater sensitivity to SRC than electron scattering cross sections. The SRC effects are relevant at photon energies above 100 MeV and for proton emission angles above 80 degrees. Unfortunately, in these kinematics, also the MEC play an important role, and their effects hide those of the SRC. For these reasons we find interesting to investigate the possibility of disentangling MEC and SRC with polarization observables.

The paper is organized as follows. In Sect. II we briefly define the observables we want to study, and present the basic ideas of our model. In Sect. III we show our results and discuss separately the effects of the FSI, of the SRC and of the MEC. Finally, in Sect. IV we summarize our findings and draw our conclusions.

## II. THE NUCLEAR MODEL

We describe a process where a proton of momentum  $\mathbf{p}$  is emitted from a nucleus after the absorption of a linearly polarized photon of momentum  $\mathbf{q}$  and energy  $\omega$ . The geometry of the process is presented in Fig. 1. We indicate with  $\phi_s$  the angle between the spin and the momentum of the photon and with  $\theta$  the angle between the  $\mathbf{q}$  and  $\mathbf{p}$  vectors. The cross section for this process can be written as [1, 11]:

$$\frac{d\sigma(\omega, \phi_s, \mathbf{p})}{d\theta} = \frac{2\pi^2 e^2}{\omega} \frac{|\mathbf{p}| m_p}{(2\pi)^3} [W_T(\omega, \omega, \mathbf{p}) + W_{TT}(\omega, \omega, \mathbf{p}) \cos \phi_s], \quad (1)$$

where  $m_p$  is the proton mass and the nuclear responses  $W_T$  and  $W_{TT}$  are defined as:

$$W_T(q, \omega, \mathbf{p}) = \sum_{\eta=\pm 1} |\langle \Psi_f(\mathbf{p}) | J_\eta(q) | \Psi_i \rangle|^2 \delta(E_f - E_i - \omega), \quad (2)$$

$$W_{TT}(q, \omega, \mathbf{p}) = 2Re \left( \langle \Psi_i | J_{+1}^\dagger(q) | \Psi_f(\mathbf{p}) \rangle \langle \Psi_f(\mathbf{p}) | J_{-1}(q) | \Psi_i \rangle \right) \delta(E_f - E_i - \omega). \quad (3)$$

In the above equations  $|\Psi_i\rangle$  and  $|\Psi_f(\mathbf{p})\rangle$  indicate the initial and final states of the nuclear system, with energies  $E_i$  and  $E_f$  respectively. Since we deal with real photons we have that, in natural units,  $\omega = E_f - E_i = |\mathbf{q}| \equiv q$ , and only the transverse components of the nuclear current  $J_{\pm 1}$  are active:

$$J_{\pm 1} = \mp \frac{1}{\sqrt{2}} (J_x \pm iJ_y). \quad (4)$$

In electron scattering there is an additional contribution to the electromagnetic current, a longitudinal term, related to the nuclear charge distribution.

In our calculations we have considered only the situations where the spin of the photon is parallel or orthogonal to  $\mathbf{q}$ . We call respectively  $\sigma_{\parallel}$  and  $\sigma_{\perp}$  the cross sections of these two cases. We have studied the photon asymmetry defined as [11]:

$$\Sigma = \frac{\sigma_{\parallel} - \sigma_{\perp}}{\sigma_{\parallel} + \sigma_{\perp}} = \frac{W_{TT}}{W_T}. \quad (5)$$

A linearly polarized photon gives information on the structure function  $W_{TT}$ , which does not contribute to the unpolarized cross section. The asymmetry  $\Sigma$  can be thought as the correction factor needed to obtain the polarized cross section ( $\sigma_{\text{pol}}$ ) from the unpolarized one ( $\sigma_{\text{unpol}}$ ), i.e.,

$$\sigma_{\text{pol}} = \sigma_{\text{unpol}} (1 + \Sigma \cos 2\phi_s). \quad (6)$$

Since  $W_T$  is always positive, the sign of the asymmetry is the sign of the structure function  $W_{TT}$ .

We have restricted our calculations to doubly closed shell nuclei; then, the nuclear ground state has zero angular momentum and positive parity, i.e.,  $|\Psi_i\rangle = |J_i M_i; \Pi_i\rangle = |00; +1\rangle$ . We describe the ground state as a Slater determinant

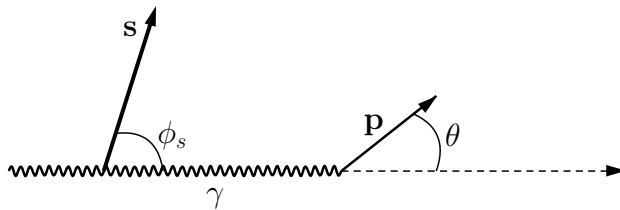


FIG. 1: Geometry of the process. We call  $\phi_s$  the angle between the directions of the spin and of the momentum of the photon. The angle  $\theta$  defines the proton emission direction with respect to the photon momentum.

of single-particle wave functions produced by a mean-field potential of Woods-Saxon type with the parameters given in Ref. [30] for  $^{12}\text{C}$  and Ref. [31] for  $^{16}\text{O}$  and  $^{40}\text{Ca}$ . We write the nuclear final state as [32]:

$$|\Psi_f\rangle = \frac{4\pi}{|p|} \sum_{l_p \mu_p} \sum_{j_p m_p} \sum_{JM, \Pi} i^{l_p} Y_{l_p \mu_p}(\hat{p}) \langle l_p \mu_p \frac{1}{2} \sigma | j_p m_p \rangle \times \langle j_p m_p j_h m_h | JM \rangle |\Psi; JM; \Pi; (l_p j_p m_p \epsilon_p, l_h j_h m_h \epsilon_h)\rangle. \quad (7)$$

In the above equation,  $|JM; \Pi; (l_p j_p m_p \epsilon_p, l_h j_h m_h \epsilon_h)\rangle$  describes the excited state of the  $A$  nucleons system with total angular momentum  $J$ ,  $z$ -axis projection  $M$ , and parity  $\Pi$ . This state is composed by a particle in a continuum wave, with orbital and total angular momenta  $l_p$  and  $j_p$  respectively, projection  $m_p$ , energy  $\epsilon_p$  and momentum  $\mathbf{p}$ , and a residual nucleus with hole quantum numbers  $l_h, j_h, m_h$  and  $\epsilon_h$ . We have indicated with  $Y_{l\mu}$  the spherical harmonics and with  $\langle l_a m_a l_b m_b | JM \rangle$  the Clebsch-Gordan coefficients [33].

In our calculations the  $|JM; \Pi; (l_p j_p m_p \epsilon_p, l_h j_h m_h \epsilon_h)\rangle$  state is a Slater determinant constructed on the ground state Slater determinant by substituting the hole wave function  $|\phi_h\rangle$  with the continuum wave function  $|\phi_p\rangle$ . This continuum single particle wave function is calculated by using a complex optical potential which is supposed to take into account the FSI. With this procedure, particle and hole wave functions are not any more orthogonal. The effects of this inconsistency have been found to be negligible in the kinematics under investigation [34].

The continuum shell model above presented has been modified to take into account the SRC in both initial and final state. We have considered only the case of scalar correlation functions acting on one-body (OB) currents. Following the basic steps of the Correlated Basis Function theory, we made a cluster expansion of the transition matrix elements of Eqs. (2) and (3) to eliminate the unlinked diagrams [35]. At this point we restrict our calculations by considering all, and only, the terms linear in the correlation function. This implies the evaluation of four two-body diagrams and six three-body diagrams, for each OB operator considered. This procedure is necessary to guarantee the correct normalization of the many-body wave functions [36]. A detailed description of the SRC model can be found in [1, 23, 24].

In our calculations we have considered only the MEC terms presented in Fig. 2 generated by the exchange of a single pion. Following the model developed in Refs. [27, 28, 29] we have calculated the seagull diagram (A in Fig. 2), the pionic diagram (B in Fig. 2) and the other two  $\Delta$  currents diagrams. The expressions of the seagull and pionic

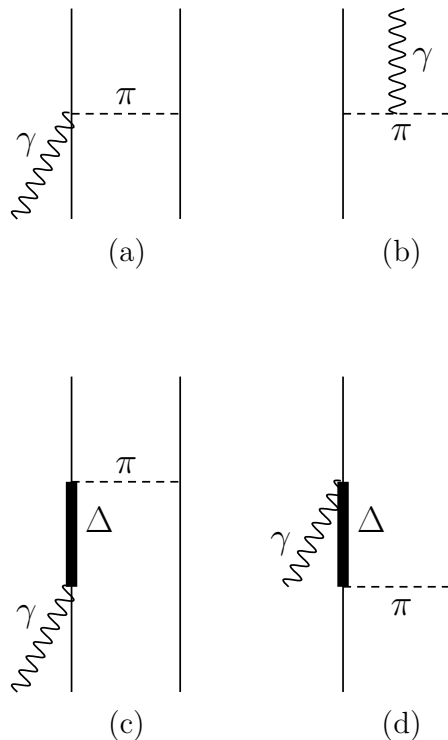


FIG. 2: Feynmann diagrams of the MEC terms considered in our calculations. The (a) and (b) diagrams represent the seagull and pionic currents, respectively, while the other two diagrams the  $\Delta$  currents.

terms are given in Ref. [1]. For the  $\Delta$  currents terms we use the following expression, more general than that used in [1]:

$$\mathbf{j}^\Delta(\mathbf{q}, \omega) = -i \frac{2}{9} \frac{f_{\pi N \Delta} f_{\pi N N} f_{\gamma N \Delta}}{m_\pi^3} \sum_{\substack{k, l=1 \\ k \neq l}}^A e^{i\mathbf{q} \cdot \mathbf{r}_k} \mathbf{q} \cdot \left\{ [\boldsymbol{\tau}(k) \times \boldsymbol{\tau}(l)]_3 \boldsymbol{\sigma}(k) \times \nabla_k \boldsymbol{\sigma}(l) \cdot \nabla_k h(\varepsilon_{kl}, \mathbf{r}_k - \mathbf{r}_l) - 4\tau^3(l) \nabla_k \boldsymbol{\sigma}(l) \cdot \nabla_k h(\varepsilon_{kl}, \mathbf{r}_k - \mathbf{r}_l) \right\} + (k \leftrightarrow l). \quad (8)$$

where  $f_{\pi N N}^2/4\pi = f_\pi^2 = 0.079$  is the effective pion-nucleon coupling constant,  $m_\pi$  is the pion mass and  $h(\mathbf{r})$  is the Fourier transform of the dynamical pion propagator [28]

$$h(\varepsilon, \mathbf{r} - \mathbf{r}_l) = \int \frac{d^3k}{(2\pi)^3} \frac{F_{\pi N}(k, \varepsilon) e^{i\mathbf{k} \cdot (\mathbf{r} - \mathbf{r}_l)}}{k^2 + m_\pi^2 - \varepsilon^2}. \quad (9)$$

We have indicated with  $F_{\pi N}$  the pion-nucleon form factor and with  $\varepsilon$  the energy of the exchanged pion. As it is clear from Fig. 2 MEC are two-body operators, then they could lead also to excited state with two particle in the continuum. We neglect their contribution which we found to be extremely small in inclusive processes [23], and we expect to be negligible also in the case under investigation. In our calculations the four single particle states involved in the MEC calculations are, the continuum state of the emitted particle, the hole state characterizing the residual nucleus, and other two states below the Fermi level. In this situation the  $\varepsilon$  energies of Eq. (9) are uniquely defined. As stated above, in our model the SRC act only on the OB currents, therefore MEC and correlations interplay only through the interference between the transition amplitudes.

### III. RESULTS

We present in this section the results of the  $(\vec{\gamma}, p)$  reaction on  $^{12}\text{C}$ ,  $^{16}\text{O}$  and  $^{40}\text{Ca}$  target nuclei. We are interested in the excitation energy region above the giant resonance and below the pion production threshold. In this region, the collective phenomena characterizing the giant resonances are not any more relevant [1], and the internal structure of the nucleon is easily parametrized. For these reasons it is plausible to attribute the corrections to a mean-field description of the process to the effects we want to study: FSI, SRC and MEC. The relevance of these effects on the asymmetry will be investigated by considering them separately. In a second step we shall present the results obtained by putting all ingredients together.

#### A. Final state interactions

We have calculated the asymmetries by using different optical potentials to describe the emitted proton wave function. In our calculations we used the potentials of Schwandt *et al.* (Sc) [37], of Comfort and Karp (CK) [38] and of Abdul-Jalil and Jackson (AJ) [39]. In addition, we have done calculations by using, also for the particle states, the same real Woods-Saxon potential considered for the hole states. We label the results of these last calculations as WS.

In Fig. 3 we show the asymmetry as a function of the proton emission angle. We fixed the photon energy at 80 MeV and we consider the  $^{12}\text{C}$ ,  $^{16}\text{O}$  and  $^{40}\text{Ca}$  nuclei. In each panel of the figure the hole state of the remaining nucleus is indicated. These calculations have been done by considering OB currents only, and without SRC. The difference between the various lines is due only to the use of different optical potentials.

The first remark is that all the asymmetries have the same order of magnitude and show similar behaviors. The differences between the various results are in the detailed structure of the angular distributions. We observe that the results obtained with the Sc and the CK optical potentials (solid and dotted lines respectively) have very similar behaviors, and show peaks roughly located at the same angle. On the contrary, the results obtained with the AJ potential (dashed curves) do not show any peak at all. Finally, the angular distributions of the WS results (dashed-dotted curves) are rather different from all the other ones.

To have a better understanding of these results, we show in Fig. 4 the  $W_T$  and  $W_{TT}$  response functions for the cases of the  $1p_{3/2}$  and  $1p_{1/2}$  hole states in  $^{16}\text{O}$ , corresponding to the panels (a) and (b) of Fig. 3. Contrary to what happens for the asymmetries, the responses have rather different sizes. For example, the WS responses are remarkably smaller than the other ones. This effect has been already discussed in [1] where we have shown that the  $(\gamma, p)$  cross sections become smaller the stronger is the real part of the particle mean-field potential.

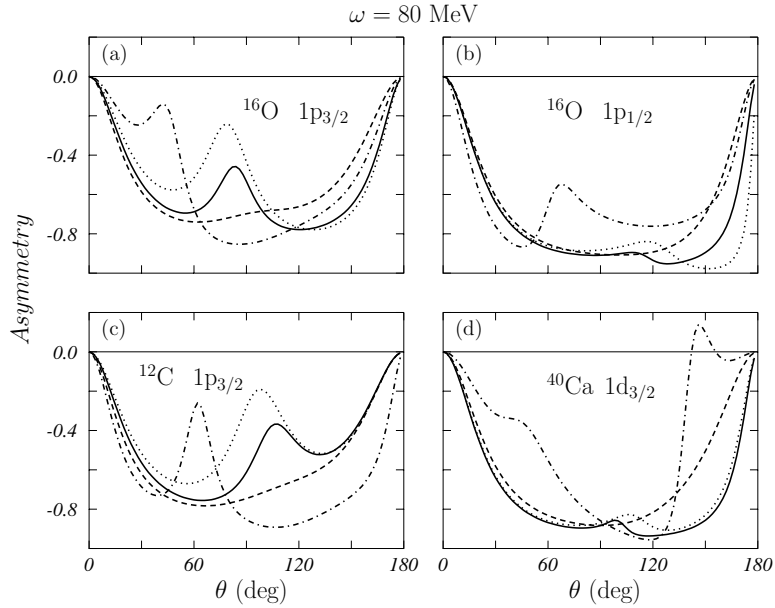


FIG. 3: Asymmetries of the  $(\bar{\gamma}, p)$  reaction, eq. (5), calculated by using OB currents only. The target nuclei and the hole states of the remaining nuclei are indicated in each panel. The photon energy has been fixed at  $\omega = 80$  MeV. The lines show the results obtained with various optical potentials. Specifically, the solid lines have been obtained with the Sc potential [37], the dotted lines with the CK potential [38], the dashed lines with the AJ potential [39], and the dashed-dotted lines with the real WS potential [30, 31].

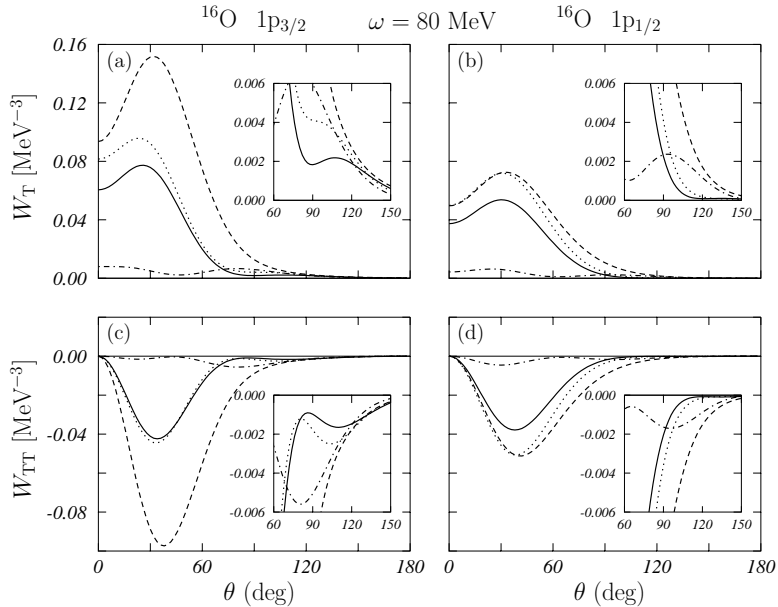


FIG. 4: The  $W_T$  (upper panels) and  $W_{TT}$  (lower panels) response functions contributing to the asymmetries for the emission from the  $1p_{3/2}$  (left panels) and  $1p_{1/2}$  (right panels) hole states. The meaning of the lines is the same as in Fig. 3. In the insert the behaviour of the responses for  $\theta \geq 60^\circ$  has been emphasized.

The shape of angular distributions of the asymmetries is characteristic of the hole state angular momentum. In Fig. 3 the results obtained for the  $1p_{3/2}$  state of  $^{16}\text{O}$  (panel (a)) and  $^{12}\text{C}$  (panel (c)) nuclei, have similar structures. They are very different from those of the  $1p_{1/2}$  state for  $^{16}\text{O}$  (panel (b)). We found similar results for the  $^{40}\text{Ca}$  hole states. Also in this case the study of the responses helps in understanding the behavior of the asymmetries. We observe in Fig. 4 that the angular distributions of the responses obtained with complex optical potentials, are rather similar. The sizes of these responses are about the same for Sc and CK. On the contrary, the AJ potential produces responses

that for the  $1p_{3/2}$  case are almost two times larger than those of the  $1p_{1/2}$  case. We found similar results for the other photon energies we have investigated.

For the  $1p_{3/2}$  hole, the CK and Sc potentials provide  $W_T$  and  $W_{TT}$  responses which show a local minimum and maximum, respectively, around 90 degrees (see inserts in panels (a) and (c)). This structure is responsible for the peak observed at this emission angle in the asymmetry (see panel (a) in Fig.3). The situation is different for the  $1p_{1/2}$  state and the asymmetry in this case (see panel (b) in Fig.3) is flat for emission angles between 60 and 150 degrees.

We can conclude that the asymmetry is less sensitive to the details of the optical potential than the cross section. The optical potential slightly modifies the shapes of the angular distributions of the asymmetries, but their sizes, and their general behaviors are almost independent from the choice of the optical potential.

The study of the  $(\gamma, p)$  cross sections [1] indicates that, in the excitation energy region we want to investigate, the Sc and CK potential provide a good description of the experimental data. These two potentials produce very similar results. For these reasons, henceforth, if not explicitly mentioned, we shall present results obtained with the Sc optical potential.

## B. Short range correlations

In this section we study the sensitivity of the asymmetries to the SRC. In our previous study of the  $(\gamma, p)$  processes [1], we found that the SRC effects become important at energies above 100 MeV and for large values of the proton emission angle. For this reason we show in Fig. 5 asymmetries calculated with photon energies of 80 (panels (a) and (b)) and also of 150 MeV (panels (c) and (d)).

The results shown in Fig. 5 have been obtained by using OB currents only. The full lines have been obtained

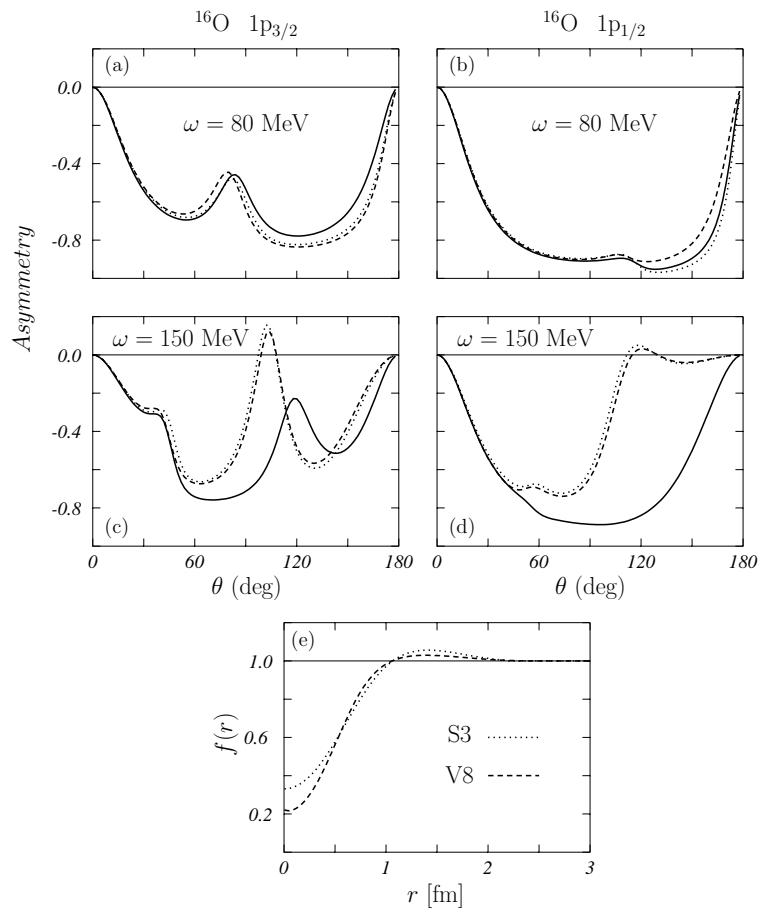


FIG. 5: Angular distribution of the asymmetries for excitation energies of 80 and 150 MeV. These results have been obtained by using OB currents only. The full lines show the results obtained without the SRC and they are the same as in Fig. 3. Dashed and dotted lines have been obtained with the correlations shown in panel (e), taken from Ref. [31] (dashed lines) and from Ref. [41] (dotted lines).

|                      | AMA   | GIU   | RYC   |
|----------------------|-------|-------|-------|
| $f_{\gamma N\Delta}$ | 0.299 | 0.373 | 0.120 |
| $f_{\pi N\Delta}$    | 1.69  | 2.15  | 2.15  |

TABLE I: Values of the parameters used in Eq. (9) for the three parameterizations considered in this work. The AMA, GIU and RYC values are from Refs. [28], [43] and [44] respectively.

without SRC. The other lines show the results obtained by using the scalar term of correlation functions taken from Fermi Hypernetted Chain calculations for finite nuclear systems. The dotted lines of Fig. 5 have been obtained with the correlation of Ref. [31] fixed to minimize the energy obtained with the semirealistic S3 nucleon-nucleon interaction of Ref. [40]. The dashed lines have been obtained by using the scalar term of the state dependent correlation function of Ref. [41]. In these last calculations the realistic Argonne  $V8'$  interaction [42] has been used. The two correlations used are shown in the panel (e) of the figure.

In agreement with Ref. [1], the effects of the SRC on the asymmetries become remarkable at high energies and for large values of the emission angle. The sensitivity of the probe is however not sufficient to disentangle the two correlation functions.

### C. Meson exchange currents

We investigate the effects of the MEC by separating the contribution of the seagull and pionic terms, corresponding to the (a) and (b) diagrams of Fig. 2, from those of the  $\Delta$  currents. The reason of this separation is that while the coupling constants related to seagull and pionic currents are well determined by pion-nucleon scattering data, the values of the  $f_{\pi N\Delta}$  and  $f_{\gamma N\Delta}$  constants, necessary to the evaluation of the  $\Delta$  currents, see Eq. 9, are still slightly uncertain. Following the procedure adopted in [25] we compare the results obtained with the three different sets of values taken from Refs. [28] (AMA), [43] (GIU) and [44] (RYC) and shown in Table I.

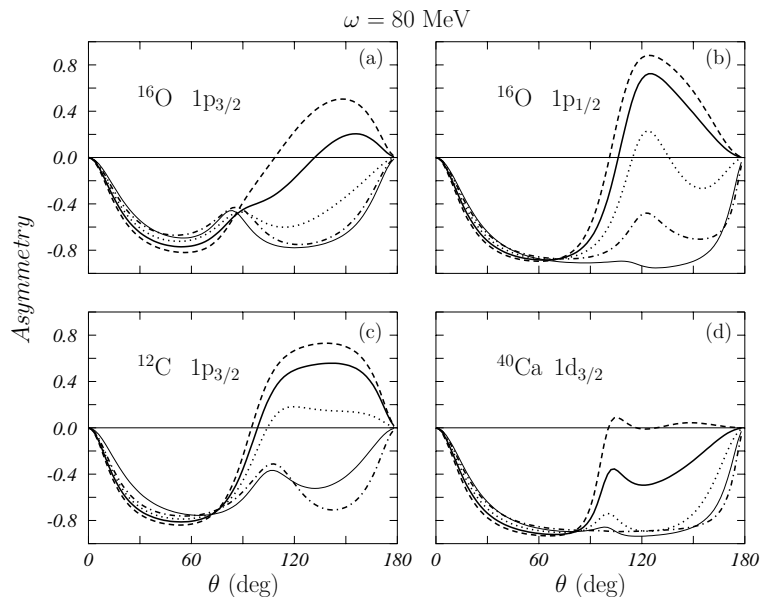


FIG. 6: Asymmetry angular distributions. The results obtained with the OB currents only, are represented by the thin solid lines. The dashed-dotted lines have been obtained by including the seagull and pionic currents. The other lines show the results obtained by including also the  $\Delta$  currents which have been calculated with the coupling constants given in Table I: AMA (thick full lines), GIU (dashed lines), RYC (dotted lines).

In Figs. 6, 7, 8 and 9, we present the angular distributions of asymmetries and responses calculated at 80 and 150 MeV. The thin solid lines show the results obtained with the OB currents only and the dashed dotted lines those obtained by including the seagull and pionic terms. The other lines have been obtained by including the  $\Delta$  currents with the three sets of parameters given in Table I. The full, dashed and dotted lines correspond to the AMA, GIU, and RYC parameterizations respectively.

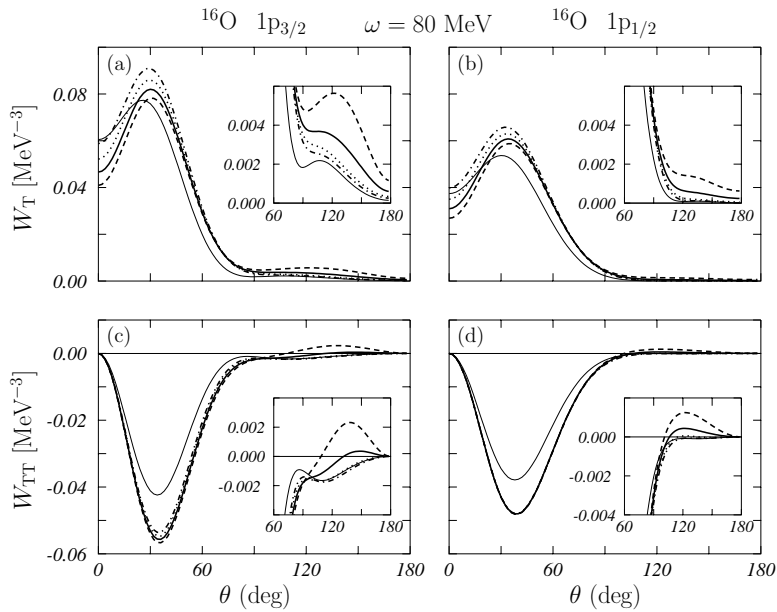


FIG. 7: Angular distributions of the  $W_T$  (upper panels) and  $W_{TT}$  (lower panels) responses. The meaning of the lines is the same as in Fig. 6.

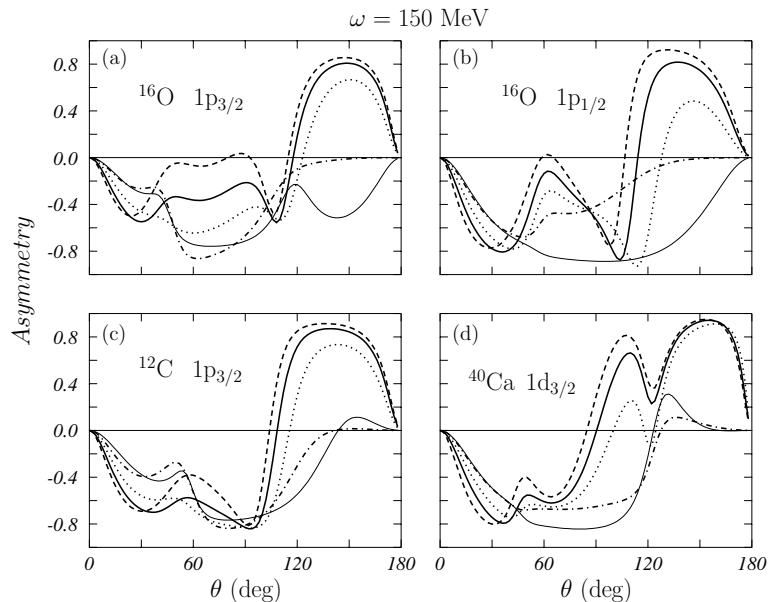


FIG. 8: The same as Fig. 6 for an excitation energy of 150 MeV.

The angular distributions of the asymmetry at 80 MeV, see Fig. 6, show that the seagull and pionic terms of the MEC produce small effects. On the contrary, the effects of the  $\Delta$  currents are remarkable. These effects are very sensitive to the values of the coupling constants and become more evident at large emission angles.

The angular distributions of the  $W_T$  and  $W_{TT}$  responses of  $^{16}\text{O}$  at 80 MeV are shown in Fig. 7. The MEC currents modify the size of minima and maxima, but in all the cases the shapes of the angular distributions are similar. There is an increase of the  $W_T$  maxima with respect to the pure OB current results. In any case, the  $\Delta$  currents lower the values obtained by including seagull and pionic terms only (dashed-dotted curves). The large effects of the MEC seen in the asymmetries are located in the region of large emission angle, where the responses are relatively small with respect to the maximum values found around  $\sim 30$  degrees. The behavior of the responses in this region is emphasized in the inserts of Fig. 7. We observe that the  $W_{TT}$  changes sign, and this produces the large effects on the asymmetries.



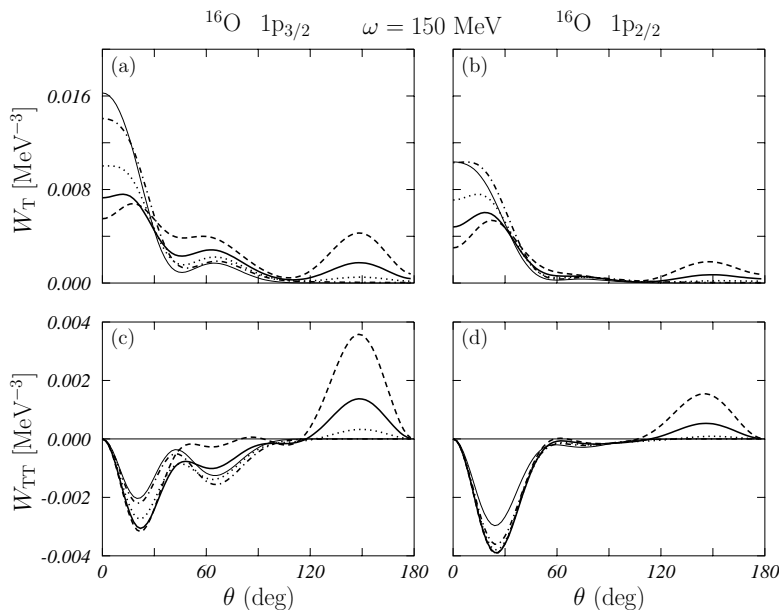


FIG. 9: The same as Fig. 7 for an excitation energy of 150 MeV.

Angular distributions of asymmetries and responses at 150 MeV are shown in Figs. 8 and 9. The asymmetries show behaviors similar to those seen at 80 MeV. The two basic facts, small effects of seagull and pionic terms, and large effects of the  $\Delta$  currents, are present also at 150 MeV. We observe much more complicated angular distribution patterns at low emission angles, and relatively large effects of seagull and pionic terms in  $^{16}\text{O}$ . The  $\Delta$  currents dominate the MEC effects, but their sensitivity to the constant values seems slightly reduced.

The study of the angular distributions of the  $W_T$  and  $W_{TT}$  terms, Fig. 9, allows a better understanding of the asymmetries behavior. It is interesting to observe that the  $W_T$  responses are peaked in the forward direction for both  $1p_{1/2}$  and  $1p_{3/2}$  emission. The inclusion of the MEC lower the values of these peaks and strongly change the shape of the distributions. On the contrary, the  $W_{TT}$  responses are not so sensitive to the presence of the MEC. Therefore the  $W_T$  responses are responsible of the large MEC effects we found in the asymmetries.

The relative effects of MEC and SRC are evident in Fig. 10 where we show asymmetries calculated at  $\theta = 120^\circ$  as a function of the excitation energy. The thin solid lines show the results obtained with OB currents only. The dotted lines show the results when the SRC correlations are included; the dashed lines have been obtained by including the MEC; the dashed-dotted lines include all terms except the contribution of the  $\Delta$  current, and the thick solid lines have been obtained by including both MEC and SRC. The parametrization AMA has been used for the  $\Delta$  current. It is evident that the dominant effect beyond the mean-field description of the process is that of the MEC. Coherence effects produced by the interference of MEC with SRC are negligible.

The behavior of the cross section at  $\theta = 120^\circ$  as a function of the excitation energy, is shown in Fig. 11. We have indicated with the full lines the unpolarized cross sections  $\sigma$ , and with the dotted and dashed lines the  $\sigma_{\parallel}$  and  $\sigma_{\perp}$ , respectively. The thin lines have been obtained by using OB currents only, while the thicker lines include also MEC and SRC. It is interesting to notice the large enhancement of the cross sections produced by the MEC in all the cases we have considered. These results are in contrast with those of Bright and Cotanch [45] which have calculated unpolarized  $(\gamma, p)$  and  $(\gamma, n)$  cross sections for  $^{16}\text{O}$ . We think that the difference is due to the description of the FSI interaction. In the calculation of Bright and Cotanch a real mean-field potential has been used. We have verified that also in our model, the use of real potential reduce the MEC effects.

#### IV. SUMMARY AND CONCLUSIONS

We have investigated polarization observables, asymmetries, in  $(\vec{\gamma}, p)$  reaction above the giant resonance region with a model which considers the contribution of the SRC and includes MEC and FSI effects. Our model has been applied to  $^{12}\text{C}$ ,  $^{16}\text{O}$  and  $^{40}\text{Ca}$  nuclei where we investigated the behavior of the asymmetries for different values of the proton scattering angle and of excitation energy.

In our investigation we found a relatively scarce sensitivity of the asymmetries to the FSI. The sizes and the

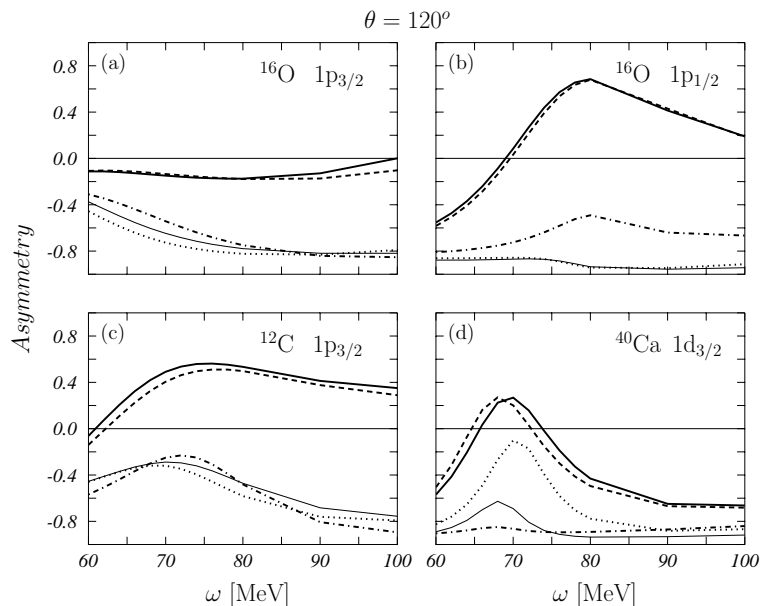


FIG. 10: Asymmetries as a function of the excitation energy for the proton emission angle  $\theta = 120^\circ$ . The full thin lines have been obtained with the OB currents only, the dotted lines by adding the SRC, the dashed lines by including MEC and the thick continuous lines by considering both MEC and SRC. The dashed-dotted lines include OB, seagull and pionic currents and SRC.

general behaviors of the asymmetries are almost independent from the choice of the optical potential. This was naively expected since the effects of the FSI factorize to a large extent in the cross sections, therefore they almost cancel in the asymmetries which are cross section ratios. Our detailed analysis shows that the details of the angular distributions depend on FSI, and they cannot be neglected.

Therefore a proper description of this observable should be done by using appropriate complex optical potentials. The importance of FSI is well known in the case of the unpolarized cross sections, but it is not so obvious for the asymmetries which are ratios of cross sections. One would have expected in this last case, that the dependence from the FSI would cancel out.

The SRC effects show up at large values of the emission angle. As in the case of the unpolarized cross sections [1], these effects are obscured by the MEC. The presence of the MEC is certainly the most important effect beyond the mean-field, one-body, description of the process. We found that the largest MEC contributions are given by the  $\Delta$  currents. We found that these contributions are already very important at energies well below the peak of the  $\Delta$  resonance. We have shown that already at 80 MeV the shapes of the asymmetries are strongly modified, at large emission angles, by the MEC. We have also shown that, always at large emission angle, the cross sections are strongly enhanced by the MEC.

While MEC effects have been clearly found in nuclear few-body systems, they are not cleanly identified in medium-heavy nuclei. We have shown that the asymmetries are extremely sensitive to the presence of MEC, in particular to the  $\Delta$  currents, which produce both quantitatively and qualitative modifications of the angular distributions. Measurements of this observable would provide clean information about MEC in medium-heavy nuclear systems.

## V. ACKNOWLEDGMENTS

This work has been partially supported by the agreement INFN-CICYT, by the spanish DGI (FIS2005-03577) and by the MURST through the PRIN: *Teoria della struttura dei nuclei e della materia nucleare*.

- 
- [1] M. Anguiano, G. Co', A. M. Lallena, and S. R. Mokhtar, Ann. Phys. (N.Y.) **296**, 235 (2002).
  - [2] R. A. Arndt, L. D. Roper, R. L. Workman, and M. W. McNaughton, Phys. Rev. D **45**, 3995 (1992).
  - [3] R. B. Wiringa, V. G. J. Stoks, and R. Schiavilla, Phys. Rev. C **51**, 38 (1995).

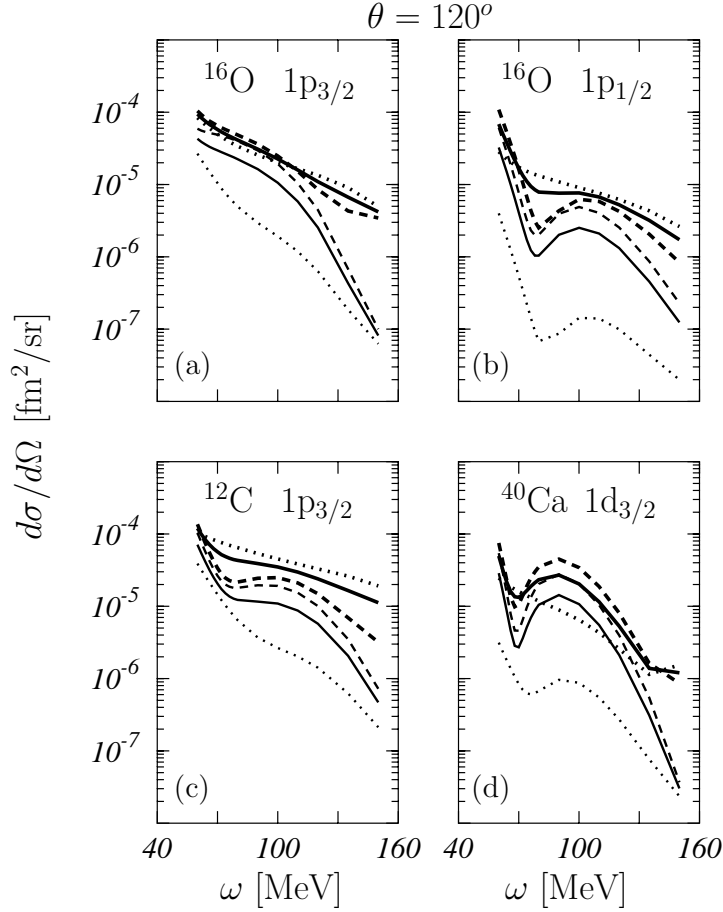


FIG. 11: Cross sections as a function of the excitation energy for a proton emission angle  $\theta = 120^\circ$ . The thin lines have been obtained by using OB currents only, and the thick lines include MEC and SRC effects. The solid, dotted and dashed lines represent the unpolarized cross section  $\sigma$ ,  $\sigma_{\parallel}$  and  $\sigma_{\perp}$ , respectively.

- [4] O. Benhar, V. R. Pandharipande, and S. C. Pieper, *Rev. Mod. Phys.* **65**, 817 (1993).
- [5] V. R. Pandharipande, I. Sick, and P. K. A. de Witt Huberts, *Rev. Mod. Phys.* **69**, 981 (1997).
- [6] J. Carlson and R. Schiavilla, *Rev. Mod. Phys.* **70**, 743 (1998).
- [7] L. E. Marcucci, M. Viviani, R. Schiavilla, A. Kievsky, and S. Rosati, *Phys. Rev. C* **72**, 014001 (2005).
- [8] S. Boffi, R. Cenni, C. Giusti, and F. D. Pacati, *Nucl. Phys. A* **420**, 38 (1984).
- [9] S. Boffi, F. Capuzzi, C. Giusti, and F. D. Pacati, *Nucl. Phys. A* **436**, 438 (1985).
- [10] S. Boffi, C. Giusti, and F. D. Pacati, *Phys. Rep. A* **226**, 1 (1993).
- [11] S. Boffi, C. Giusti, F. Pacati, and M. Radici, *Electromagnetic Response of Atomic Nuclei* (Clarendon, Oxford, 1996).
- [12] K. Wienhard, R. K. M. Schneider, K. Ackermann, K. Bangert, U. E. P. Berg, and R. Stock, *Phys. Rev. C* **24**, 1363 (1981).
- [13] J. Yokokawa et al., *J. Phys. Soc. Jpn* **57**, 695 (1988).
- [14] <http://wwwa2.kph.uni-mainz.de/A2/>.
- [15] <http://www.maxlab.lu.se/>.
- [16] G. J. Miller et al., *Nucl. Phys. A* **586**, 125 (1995).
- [17] S. Franczuk et al., *Phys. Lett. B* **450**, 332 (1999).
- [18] <http://higs.tunl.duke.edu/>.
- [19] E. C. Schreiber et al., *Phys. Rev. C* **61**, 061604(R) (2000).
- [20] G. Co' and A. M. Lallena, *Phys. Rev. C* **57**, 145 (1998).
- [21] J. E. Amaro, A. M. Lallena, G. Co', and A. Fabrocini, *Phys. Rev. C* **57**, 3473 (1998).
- [22] S. R. Mokhtar, G. Co', and A. M. Lallena, *Phys. Rev. C* **62**, 067304 (2000).
- [23] G. Co' and A. M. Lallena, *Ann. Phys. (N.Y.)* **287**, 101 (2001).
- [24] S. R. Mokhtar, M. Anguiano, G. Co', and A. M. Lallena, *Ann. Phys. (N.Y.)* **292**, 67 (2001).
- [25] M. Anguiano, G. Co', and A. M. Lallena, *Jour. Phys. G* **29**, 1119 (2003).
- [26] M. Anguiano, G. Co', and A. M. Lallena, *Nucl. Phys. A* **744**, 2004 (2004).

- [27] J. E. Amaro, G. Co', and A. M. Lallena, *Ann. Phys. (N.Y.)* **221**, 306 (1993).
- [28] J. E. Amaro, G. Co', and A. M. Lallena, *Nucl. Phys. A* **578**, 365 (1994).
- [29] J. E. Amaro, Ph.D. thesis, Universidad de Granada (Spain) (1993), unpublished.
- [30] A. Botrugno and G. Co', *Nucl. Phys. A* **761**, 203 (2005).
- [31] F. Arias de Saavedra, G. Co', A. Fabrocini, and S. Fantoni, *Nucl. Phys. A* **605**, 359 (1996).
- [32] G. Co' and S. Krewald, *Nucl. Phys. A* **433**, 392 (1985).
- [33] A. R. Edmonds, *Angular momentum in quantum mechanics* (Princeton University Press, Princeton, 1957).
- [34] S. Boffi, F. Cannata, F. Capuzzi, C. Giusti, and F. D. Pacati, *Nucl. Phys. A* **379**, 509 (1982).
- [35] S. Fantoni and V. R. Pandharipande, *Nucl. Phys. A* **473**, 234 (1987).
- [36] G. Co', *Nuov. Cim. A* **108**, 623 (1995).
- [37] P. Schwandt, H. O. Meyer, W. W. Jacobs, A. D. Bacher, S. E. Vigdor, M. D. Kaitchuck, and T. R. Donoghue, *Phys. Rev. C* **26**, 55 (1982).
- [38] J. R. Comfort and B. C. Karp, *Phys. Rev. C* **21**, 2162 (1980).
- [39] I. Abdul-Jalil and D. F. Jackson, *J. Phys. G* **6**, 481 (1980).
- [40] I. Afnan and Y. Tang, *Phys. Rev.* **175**, 1337 (1968).
- [41] C. Bisconti, F. Arias de Saavedra, G. Co', and A. Fabrocini, *Phys. Rev. C* **73**, 054304 (2006).
- [42] B. S. Pudliner, V. R. Pandharipande, J. Carlson, and R. B. Wiringa, *Phys. Rev. Lett.* **74**, 4396 (1995).
- [43] C. Giusti and F. D. Pacati, *Nucl. Phys. A* **615**, 373 (1997).
- [44] J. Ryckebusch, V. V. der Sluys, K. Heyde, H. Holvoet, W. V. Nespren, M. Waroquier, and M. Vanderhaeghen, *Nucl. Phys. A* **624**, 581 (1997).
- [45] T. B. Bright and S. R. Cotanch, *Phys. Rev. Lett.* **71**, 2563 (1993).